A&A 575, A130 (2015)
DOI: 10.1051/0004-6361/201424611

Astronomy & Astrophysics

Propagating kink waves in thin twisted magnetic tubes with continuous equilibrium magnetic field⋆

M. S. Ruderman[1,2]

[1] Solar Physics and Space Plasma Research Centre (SP²RC), University of Sheffield, Hicks Building, Hounsfield Road, Sheffield S3 7RH, UK
e-mail: m.s.ruderman@sheffield.ac.uk
[2] Space Research Institute (IKI) Russian Academy of Sciences, 117997 Moscow, Russia

Received 16 July 2014 / Accepted 21 January 2015

ABSTRACT

In this paper, we study kink waves in twisted magnetic tubes. In the equilibrium state there is the electrical current with constant density inside the tube directed along the tube axis. This current creates the azimuthal magnetic field with the magnitude proportional to the distance from the tube axis inside the tube and inversely proportional to this distance outside the tube. We derive the dispersion equations for propagating waves and for unstable perturbations in the long wavelength approximation. We show that there are no solutions to the dispersion equation determining the frequencies of unstable perturbations, which implies that there are no unstable long kink modes. We study the dispersion equation for propagating waves both in the case when the plasma density is larger than that in the surrounding plasma as well as when it is smaller. In the first case we obtain that, depending on the wave number, the dispersion equation for propagating waves has either no solutions, or one solution, or two solutions. In the case when there is one solution, in the approximation of very weak twist, the wave mode propagates with the phase speed slightly larger than the kink speed. This wave mode is called the accelerated kink wave. In the case when there are two solutions to the dispersion equation, one of the two solutions gives the frequency of a quasi-mode that is subjected to the Alfvén resonance outside the tube. The other solution gives the frequency of a true eigenmode of linear ideal MHD. In the approximation of very weak twist its phase speed is smaller than the kink speed. This mode is called the decelerated kink wave. In the case of rarefied tube, depending on the wave number, the dispersion equation has either one or three solutions. When there is only one solution, the mode frequency is very close to the Alfvén frequency far from the tube, so the wave mode practically coincides with the Alfvén wave. When there are three solutions, the largest frequency practically coincides with the Alfvén frequency far from the tube. Two other solutions almost coincide. In all cases the wave modes existing in the case of rarefied tube are quasi-modes that are subjected to the Alfvén resonance. A possible application of the obtained results to the solar atmospheric seismology is discussed.

Key words. magnetohydrodynamics (MHD) – plasmas – waves – methods: analytical – instabilities – magnetic fields

1. Introduction

Since transverse oscillations of coronal magnetic loops were first detected by TRACE and interpreted as fast standing kink waves (Aschwanden et al. 1999; Nakariakov et al. 1999), they continue to receive ample attention of solar physicists. Later propagating kink waves have been observed in coronal loops (Tomczyk et al. 2007; Tomczyk & McIntosh 2009; Pascoe et al. 2010), in spicules (De Pontieu et al. 2007; He et al. 2009a,b), in the fine structure of prominences (Okamoto et al. 2007), and in filament threads (Lin et al. 2007, 2009). Recently, Morton et al. (2012) reported observations of the simultaneous propagation of kink and sausage waves in a chromospheric magnetic wave guide. In the first theoretical interpretation of kink waves in coronal loops, a very simple model of a coronal magnetic loop, which is a straight magnetic tube, was used (e.g. Ryutov & Ryutova 1976; Edwin & Roberts 1983). More sophisticated models have been developed later. For a review of theory of the coronal loop oscillations see, e.g. Ruderman & Erdélyi (2009).

The numerous observations of propagating kink waves prompted a number of theoretical studies of these waves. In particular, the damping of these waves was studied (Pascoe et al. 2010, 2011, 2012; Ruderman et al. 2010; Terradas et al. 2010; Soler et al. 2008; Hood et al. 2013), the energy flux in the magnetic flux tube was calculated (Goossens et al. 2013), and possible Doppler signatures of propagating kink waves were analysed (Goossens et al. 2014).

One important problem in the theory of coronal loop kink oscillations is the effect of magnetic twist. Twisted magnetic tubes have been studied for many years in the context of the tube stability (e.g. Dungey & Loughead 1954; Roberts 1956; Shafranov 1957; Kruskal & Tuck 1958; Parker 1974; Browning & Priest 1983). They have also been studied in relation to the magnetohydrodynamic (MHD) wave resonant absorption (e.g. Sakurai et al. 1991; Goossens & Ruderman 1995; Goossens et al. 1995; Ballay & Erdélyi 2002). Wave propagation in twisted magnetic tubes has been investigated by Bogdan (1984), Bennett et al. (1999), Erdélyi & Carter (2006), Carter & Erdélyi (2007), and Erdélyi & Fedun (2007).

Ruderman (2007, Paper I) considered kink waves in a thin twisted magnetic tube with a purely axial magnetic field outside the tube and the azimuthal component of the magnetic field proportional to the radial distance from the tube axis inside the tube. Although Paper I mainly dealt with standing waves, the equation

⋆ Appendices are available in electronic form at http://www.aanda.org

governing the waves that was derived also describes propagating waves. Terradas & Goossens (2012) studied the standing kink waves in a magnetic tube with the magnetic twist confined to an annulus inside the tube.

In the magnetic tube considered in Paper I, the magnetic field is discontinuous at the tube boundary, meaning that there is the surface current at this boundary. In this paper we aim to study kink waves in a magnetic tube with a more realistic equilibrium magnetic field that is continuous at the tube boundary. We only consider propagating waves. Standing waves are studied in an accompanying paper.

The paper is organized as follows: in the next section we formulate the problem and present the governing equations and boundary conditions. In Sect. 3 we derive the dispersion equations determining the frequencies of propagating waves and unstable perturbations. In Sect. 4 we investigate the properties of propagating waves. Section 5 contains the summary of the results and our conclusions.

2. Equilibrium state and governing equations

We consider a twisted magnetic tube of radius a.The equilibrium plasma density is assumed to be constant inside and outside the tube. Hence, in cylindrical coordinates r, φ, z with the z-axis coinciding with the tube axis, it is given by

$$\rho = \begin{cases} \rho_{\rm i}, & r < a, \\ \rho_{\rm e}, & r > a, \end{cases} \tag{1}$$

where $\rho_{\rm i}$ and $\rho_{\rm e}$ are constant. Observations show that in coronal loops $\rho_{\rm i} > \rho_{\rm e}$. However, in waveguides in the chromosphere the opposite inequality can be satisfied. The only condition that we impose on the plasma density here therefore is $\rho_{\rm i} \neq \rho_{\rm e}$. We assume that there is electrical current with constant density directed along the tube axis. This electrical current creates the azimuthal magnetic field with the magnitude proportional to r inside the tube and to $1/r$ outside. The equilibrium magnetic field only depends on r and has two components, axial, B_z, and azimuthal, B_φ. We use the cold plasma approximation throughout, therefore the equilibrium magnetic field must be force-free. This condition reduces to

$$\frac{{\rm d}B^2}{{\rm d}r} = -\frac{2B_\varphi^2}{r}, \tag{2}$$

where $B^2 = B_\varphi^2 + B_z^2$. We use the subscripts "i" and "e" to distinguish between quantities inside and outside the tube. We drop these indices when there is no danger of confusion. We assume that $B_{z\rm e}$ is constant, $B_{\varphi\rm i}$ is proportional to r, $B_{\varphi\rm e}$ is inversely proportional to r, and the magnetic field is continuous at $r = a$. Then, using Eq. (2), we obtain that the equilibrium magnetic field is given by

$$B_z^2 = \begin{cases} B_0^2 + 2A^2(a^2 - r^2), & r < a, \\ B_0^2, & r > a, \end{cases} \qquad B_\varphi = \begin{cases} Ar, & r < a, \\ a^2 A/r, & r > a, \end{cases} \tag{3}$$

where A and B_0 are positive constants, and we assume that $B_z > 0$.

The plasma motion is described by the linearised ideal MHD equations for cold plasmas,

$$\rho' = -\nabla \cdot (\rho \boldsymbol{\xi}) = 0, \tag{4}$$

$$\rho \frac{\partial^2 \boldsymbol{\xi}}{\partial t^2} = \frac{1}{\mu_0}(\nabla \times \boldsymbol{b}) \times \boldsymbol{B} + \frac{1}{\mu_0}(\nabla \times \boldsymbol{B}) \times \boldsymbol{b}, \tag{5}$$

$$\boldsymbol{b} = \nabla \times (\boldsymbol{\xi} \times \boldsymbol{B}). \tag{6}$$

Here $\boldsymbol{\xi}$ is the plasma displacement related to the plasma velocity $\boldsymbol{u}$ by $\boldsymbol{u} = \partial\boldsymbol{\xi}/\partial t$, $\boldsymbol{b}$ the magnetic field perturbation, ρ' the density perturbation, $\boldsymbol{B}$ the background magnetic field, ρ the background plasma density, and μ_0 the magnetic permeability of free space.

Equation (4), which defines the density perturbation, is not used below. It has been shown in Paper I that Eqs. (5) and (6) can be transformed to

$$\rho \frac{\partial^2 \xi_r}{\partial t^2} = -\frac{\partial P}{\partial r} + \frac{B}{\mu_0}\mathcal{D}_\parallel b_r - \frac{2B_\varphi b_\varphi}{r\mu_0}, \tag{7}$$

$$\rho \frac{\partial^2 \xi_\perp}{\partial t^2} = -\mathcal{D}_\perp P + \frac{B}{\mu_0}\mathcal{D}_\parallel b_\perp + \frac{b_r}{\mu_0}\left[\frac{B_z}{rB}\frac{{\rm d}(rB_\varphi)}{{\rm d}r} - \frac{B_\varphi}{B}\frac{{\rm d}B_z}{{\rm d}r}\right], \tag{8}$$

$$b_r = B\mathcal{D}_\parallel \xi_r, \tag{9}$$

$$b_\perp = B\mathcal{D}_\parallel \xi_\perp + \xi_r\left[\frac{B_\varphi}{rB}\frac{{\rm d}(rB_z)}{{\rm d}r} - \frac{B_z}{B}\frac{{\rm d}B_\varphi}{{\rm d}r}\right], \tag{10}$$

$$P = -\frac{B_\varphi}{\mu_0}\frac{\partial(\xi_r B_\varphi)}{\partial r} - \frac{B_z}{r\mu_0}\frac{\partial(r\xi_r B_z)}{\partial r} - \frac{B^2}{\mu_0}\mathcal{D}_\perp \xi_\perp. \tag{11}$$

Here $P = (B_\varphi b_\varphi + B_z b_z)/\mu_0$ is the magnetic pressure perturbation, $\xi_\perp = (B_z\xi_\varphi - B_\varphi\xi_z)/B$, and $b_\perp = (B_z b_\varphi - B_\varphi b_z)/B$. The operators $\mathcal{D}_\perp$ and $\mathcal{D}_\parallel$ are determined by

$$\mathcal{D}_\perp = \frac{B_z}{rB}\frac{\partial}{\partial\varphi} - \frac{B_\varphi}{B}\frac{\partial}{\partial z}, \quad \mathcal{D}_\parallel = \frac{B_\varphi}{rB}\frac{\partial}{\partial\varphi} + \frac{B_z}{B}\frac{\partial}{\partial z}. \tag{12}$$

Note that the component of the plasma displacement that is parallel to the equilibrium magnetic field, $\xi_\parallel = (B_\varphi\xi_\varphi + B_z\xi_z)/B$, is equal to zero in the cold-plasma approximation.

Equations (7)–(11) have to be supplemented with the kinematic and dynamic boundary conditions at the tube boundary. The kinematic boundary condition states that the radial plasma displacement has to be continuous,

$$\xi_{r\rm i} = \xi_{r\rm e} \quad \text{at} \quad r = a. \tag{13}$$

Because both the plasma displacement in the radial direction and the azimuthal magnetic field are continuous at the tube boundary, the dynamic boundary condition reduces to

$$P_{\rm i} = P_{\rm e} \quad \text{at} \quad r = a. \tag{14}$$

Finally, all perturbations have to vanish as $r \to \infty$. Equations (7)–(11) together with the boundary conditions (13) and (14) are used in the next section to derive the dispersion equations for kink waves and unstable perturbations in the magnetic tube.

3. Deriving the dispersion equations

In this section, we derive the dispersion equations that determine the frequency of kink perturbations. We take all variables proportional to $\mathrm{e}^{{\rm i}m\varphi}$, where $|m| = 1$. We only consider long waves and assume that the tube is thin, $a/l = \epsilon \ll 1$, where l is the wavelength. In accordance with this we introduce the scaled variable in the z-direction, $Z = \epsilon z$. The phase speed of kink waves is of the order of $V_{\rm A} = B_0(\mu_0\rho_{\rm i})^{-1/2}$, so the characteristic Alfvénic time is $a/V_{\rm A}$. On the other hand, the characteristic period of kink waves is $l/V_{\rm A}$. This estimate suggests introducing the scaled time $T = \epsilon t$. To satisfy the Shafranov-Kruskal stability criterion (e.g. Roberts 1956; Shafranov 1957; Kruskal & Tuck 1958), similar to Paper I, we assume that $A = \epsilon\widetilde{A}$ with $\widetilde{A} \lesssim B_0/a$. This assumption also agrees very well with observations that showed that the azimuthal component of the magnetic field in

coronal magnetic loops is much smaller than the axial component. We perfome the Fourier analysis of the perturbations with respect to Z and consider perturbations in the form of normal modes. In accordance with this, we take perturbations of all variables proportional to $\exp[\mathrm{i}(KZ - \Omega T)]$.

Now, eliminating b_r and $b_\perp$ from Eqs. (7)–(11), we reduce this system of equations to equations for ξ_r, $\xi_\perp$ and P:

$$\left(\Omega^2 - \Omega_\mathrm{A}^2\right)\xi_r + \frac{2\widetilde{B}_\varphi}{r\mu_0\rho}\frac{\mathrm{d}(\widetilde{B}_\varphi\xi_r)}{\mathrm{d}r} = \frac{\epsilon^{-2}}{\rho}\frac{\mathrm{d}P}{\mathrm{d}r} + \frac{2\mathrm{i}B\widetilde{B}_\varphi K}{r\mu_0\rho}\xi_\perp + O\left(\epsilon^2\right), \tag{15}$$

$$\left(\Omega^2 - \Omega_\mathrm{A}^2\right)\xi_\perp = \frac{\mathrm{i}\epsilon^{-2}}{F}P + \frac{2\widetilde{B}_\varphi\Omega_\mathrm{A}}{r\sqrt{\mu_0\rho}}\xi_r + O\left(\epsilon^2\right), \tag{16}$$

$$P = -\frac{B^2}{r\mu_0}\frac{\mathrm{d}(r\xi_r)}{\mathrm{d}r} + \frac{2\epsilon^2\widetilde{B}_\varphi^2}{r\mu_0}\xi_r - \frac{\mathrm{i}B^2F}{\mu_0}\xi_\perp. \tag{17}$$

Here $\widetilde{B}_\varphi = \epsilon^{-1}B_\varphi$,

$$\Omega_\mathrm{A} = \frac{1}{\sqrt{\mu_0\rho}}\left(\frac{m\widetilde{B}_\varphi}{r} + B_0K\right), \quad F = \frac{mB_z}{rB} - \frac{\epsilon^2\widetilde{B}_\varphi K}{B_0}. \tag{18}$$

Since we consider a static equilibrium, it follows from the general spectral theory of the linear ideal MHD that the square of the eigenfrequency is always real, but it can either be positive or negative (e.g. Goedbloed & Poedts 2004). We here consider both cases.

Substituting the expression for P given by Eq. (17) in Eqs. (16), we obtain

$$F\left[F\xi_\perp - \frac{\mathrm{i}}{r}\frac{\mathrm{d}(r\xi_r)}{\mathrm{d}r}\right] = \epsilon^2\frac{\mu_0\rho}{B_0^2}\left(\Omega^2 - \Omega_\mathrm{A}^2\right)\xi_\perp + \epsilon^2\frac{2\mathrm{i}\widetilde{B}_\varphi K}{rB_0}\xi_r + O(\epsilon^4). \tag{19}$$

We consider this equation as an equation for $\xi_\perp$ and search for the solution in the form of the series expansion with respect to ϵ^2,

$$\xi_\perp = \xi_\perp^{(0)} + \epsilon^2\xi_\perp^{(1)} + \ldots \tag{20}$$

After calculating the solution to Eq. (19), we substitute it in Eq. (17) to obtain the expression for P in terms of ξ_r. Substituting this expression and expression for $\xi_\perp$ in Eq. (15) we obtain the equation for ξ_r and solve it. Then we express P in terms of ξ_r. We carry out this procedure separately in the internal ($r < a$) and external ($r > a$) region.

3.1. Solution inside the tube

Using Eqs. (1) and (3), we write Eqs. (15), (17) and (19) in the internal region as

$$\left(\Omega^2 - \Omega_\mathrm{Ai}^2\right)\xi_r + \frac{2\widetilde{A}^2}{\mu_0\rho_\mathrm{i}}\frac{\mathrm{d}(r\xi_r)}{\mathrm{d}r} = \frac{\epsilon^{-2}}{\rho_\mathrm{i}}\frac{\mathrm{d}P}{\mathrm{d}r} + \frac{2\mathrm{i}B_0\widetilde{A}K}{\mu_0\rho_\mathrm{i}}\xi_\perp + O\left(\epsilon^2\right), \tag{21}$$

$$P = -\frac{B_\mathrm{i}^2}{r\mu_0}\frac{\mathrm{d}(r\xi_r)}{\mathrm{d}r} + \frac{2\epsilon^2r\widetilde{A}^2}{\mu_0}\xi_r - \frac{\mathrm{i}B_\mathrm{i}^2F_\mathrm{i}}{\mu_0}\xi_\perp + O\left(\epsilon^4\right), \tag{22}$$

$$F_\mathrm{i}\left[F_\mathrm{i}\xi_\perp - \frac{\mathrm{i}}{r}\frac{\mathrm{d}(r\xi_r)}{\mathrm{d}r}\right] = \epsilon^2\frac{\mu_0\rho_\mathrm{i}}{B_0^2}\left(\Omega^2 - \Omega_\mathrm{Ai}^2\right)\xi_\perp + \epsilon^2\frac{2\mathrm{i}\widetilde{A}K}{B_0}\xi_r + O\left(\epsilon^4\right), \tag{23}$$

where

$$\Omega_\mathrm{Ai} = \frac{m\widetilde{A} + B_0K}{\sqrt{\mu_0\rho_\mathrm{i}}}, \quad F_\mathrm{i} = \frac{mB_{z\mathrm{i}}}{rB_\mathrm{i}} - \frac{\epsilon^2r\widetilde{A}K}{B_0}. \tag{24}$$

Below, we also use the expansions

$$B_{z\mathrm{i}} = B_0 + \epsilon^2\widetilde{A}^2\frac{a^2 - r^2}{B_0} + O\left(\epsilon^4\right), \quad B_\mathrm{i} = B_0 + \epsilon^2\widetilde{A}^2\frac{2a^2 - r^2}{2B_0} + O\left(\epsilon^4\right). \tag{25}$$

In the first-order approximation we collect terms of the order of unity in Eq. (23). As a result, we obtain

$$\xi_\perp^{(0)} = \frac{\mathrm{i}}{m}\frac{\mathrm{d}(r\xi_r)}{\mathrm{d}r}. \tag{26}$$

In the next order approximation we collect terms of the order of ϵ^2 in Eq. (23). Then, using Eqs. (24)–(26), we obtain

$$\xi_\perp^{(1)} = \frac{\mathrm{i}mr^2}{2}\left[\frac{\mu_0\rho_\mathrm{i}(2\Omega^2 - \Omega_\mathrm{Ai}^2)}{B_0^2} - K^2\right]\frac{\mathrm{d}(r\xi_r)}{\mathrm{d}r} + \frac{2\mathrm{i}r^2\widetilde{A}K}{B_0}\xi_r. \tag{27}$$

Substituting Eqs. (26) and (27) in Eq. (22) and using Eq. (24) yields

$$\epsilon^{-2}P = r\rho_\mathrm{i}\left[m\left(\Omega^2 - \Omega_\mathrm{Ai}^2\right)\frac{\mathrm{d}(r\xi_r)}{\mathrm{d}r} + \frac{2\widetilde{A}\Omega_\mathrm{Ai}}{\sqrt{\mu_0\rho_\mathrm{i}}}\xi_r\right] + O\left(\epsilon^2\right). \tag{28}$$

Substituting Eqs. (26) and (28) in Eq. (21) and collecting terms of the order of unity in the obtained equation we obtain the equation for ξ_r valid in the leading-order approximation with respect to ϵ^2:

$$\left(\Omega^2 - \Omega_\mathrm{Ai}^2\right)\left(r^2\frac{\mathrm{d}^2\xi_r}{\mathrm{d}r^2} + 3r\frac{\mathrm{d}\xi_r}{\mathrm{d}r}\right) = 0. \tag{29}$$

Equation $\Omega^2 = \Omega_\mathrm{Ai}^2$ describes Alfvén waves inside the tube. We exclude these waves from the analysis. This implies that the expression in the second pair of brackets in Eq. (29) is zero. Then the solution to Eq. (29) regular at $r = 0$ is

$$\xi_r = \eta, \tag{30}$$

where η is an arbitrary constant. Substituting this result in Eq. (28) we obtain, again in the leading-order approximation,

$$P = \epsilon^2a\eta\rho_\mathrm{i}\left(\Omega^2 - \frac{B_0^2K^2 - \widetilde{A}^2}{\mu_0\rho_\mathrm{i}}\right). \tag{31}$$

3.2. Solution in the external region

While the characteristic scale in the radial direction in the tube is a, this is, in general, not true outside the tube. In the whole external region this characteristic scale is l. However, the external region can be divided into two parts: the inner external region defined by the condition $r \sim a$, and the outer external region defined by the condition $r \gg a$. The characteristic scale in the radial direction in the inner external region is still equal to a, so we can use Eqs. (15)–(17) to describe the plasma motion in this region. In the outer external region we have to introduce the new scaled variable $R = \epsilon r$. Then we can obtain the solution in the external region using the method of matched asymptotic expansions. In accordance with this method we obtain the solution in the inner and outer external region separately, and then

match the two solutions in the overlap region defined by the condition $a \ll r \ll l$.

The solution in the outer external region is not used to derive the dispersion equation. All that we need from this solution is the boundary condition for the solution in the inner external region that is imposed by the matching conditions. In accordance with the matching conditions the asymptotic expression for the solution in the inner external region valid for large r has to coincide with the asymptotic expression for the solution in the outer external region valid for small R. Since B_φ is inversely proportional to r, it can be neglected in the outer external region and the magnetic field in this region can be considered as approximately homogeneous and in the z-direction. The solution describing the plasma motion in the presence of such an equilibrium magnetic field was obtained, for example, in Paper I. In this solution, $P \propto R^{-1}$ and $\xi_r \propto R^{-2}$ for small R. Then the matching conditions imply that the asymptotic behaviour of the solution in the inner external region for large r has to be $P \propto r^{-1}$ and $\xi_r \propto r^{-2}$. In accordance with this, we determine the solution in the inner external region that vanishes as $r \to \infty$ below.

Using Eqs. (1) and (3), we write Eqs. (15), (17) and (19) in the external region as

$$\left(\Omega^2 - \Omega_{\rm Ae}^2\right)\xi_r + \frac{2a^4\widetilde{A}^2}{\mu_0\rho_{\rm e}r^2}\frac{\mathrm{d}}{\mathrm{d}r}\left(\frac{\xi_r}{r}\right) = \frac{\epsilon^{-2}}{\rho_{\rm e}}\frac{\mathrm{d}P}{\mathrm{d}r} + \frac{2\mathrm{i}a^2B_0\widetilde{A}K}{\mu_0\rho_{\rm e}r^2}\xi_\perp + O\left(\epsilon^2\right), \quad (32)$$

$$P = -\frac{B_{\rm e}^2}{r\mu_0}\frac{\mathrm{d}(r\xi_r)}{\mathrm{d}r} + \frac{2\epsilon^2a^4\widetilde{A}^2}{\mu_0r^3}\xi_r - \frac{\mathrm{i}B_{\rm e}^2F_{\rm e}}{\mu_0}\xi_\perp, \quad (33)$$

$$F_{\rm e}\left[F_{\rm e}\xi_\perp - \frac{i}{r}\frac{\mathrm{d}(r\xi_r)}{\mathrm{d}r}\right] = \epsilon^2\frac{\mu_0\rho_{\rm e}}{B_0^2}\left(\Omega^2 - \Omega_{\rm Ae}^2\right)\xi_\perp + \epsilon^2\frac{2\mathrm{i}a^2\widetilde{A}K}{r^2B_0}\xi_r + O\left(\epsilon^4\right), \quad (34)$$

where

$$\Omega_{\rm Ae} = \frac{1}{\sqrt{\mu_0\rho_{\rm e}}}\left(\frac{ma^2\widetilde{A}}{r^2} + B_0K\right), \quad F_{\rm e} = \frac{mB_0}{rB_{\rm e}} - \frac{\epsilon^2a^2\widetilde{A}K}{rB_0}. \quad (35)$$

We also use the expansion

$$B_{\rm e} = B_0 + \epsilon^2\frac{a^4\widetilde{A}^2}{2r^2B_0} + O\left(\epsilon^4\right). \quad (36)$$

In the first-order approximation the solution to Eq. (34) is again given by Eq. (26). In the next order approximation we obtain

$$\xi_\perp^{(1)} = \mathrm{i}mr^2\left[\frac{\mu_0\rho_{\rm e}(2\Omega^2 - \Omega_{\rm Ae}^2)}{B_0^2} - K^2\right]\frac{\mathrm{d}(r\xi_r)}{\mathrm{d}r} + \frac{2\mathrm{i}a^2\widetilde{A}K}{B_0}\xi_r. \quad (37)$$

Substituting Eqs. (35)–(37) in Eq. (33) yields

$$\epsilon^{-2}P = r\rho_{\rm e}\left[\left(\Omega^2 - \Omega_{\rm Ae}^2\right)\frac{\mathrm{d}(r\xi_r)}{\mathrm{d}r} + \frac{2ma^2\widetilde{A}\Omega_{\rm Ae}}{r^2\sqrt{\mu_0\rho_{\rm e}}}\xi_r\right] + O\left(\epsilon^2\right). \quad (38)$$

Collecting terms of the order of unity in Eq. (32) and using Eqs. (26) and (38) we obtain, after some algebra, the equation for ξ_r valid in the leading-order approximation with respect to ϵ^2:

$$\frac{\mathrm{d}}{\mathrm{d}r}\left[r^3\left(\Omega^2 - \Omega_{\rm Ae}^2\right)\frac{\mathrm{d}\xi_r}{\mathrm{d}r}\right] = 0. \quad (39)$$

It follows from this equation that

$$r^3\left[\Omega^2 - \frac{1}{\mu_0\rho_{\rm e}}\left(\frac{ma^2\widetilde{A}}{r^2} + B_0K\right)^2\right]\frac{\mathrm{d}\xi_r}{\mathrm{d}r} = \chi = \text{const}. \quad (40)$$

Below we only consider trapped waves with frequencies smaller than the Alfvén frequency at $r \gg a$. Hence, we impose the condition

$$|\Omega| < \frac{B_0|K|}{\mu_0\rho_{\rm e}} \quad (41)$$

when $\Omega^2 > 0$. Then, integrating Eq. (40) and taking into account that $\xi_r \to 0$ as $r \to \infty$ we obtain

$$\xi_r = \frac{m\chi\sqrt{\mu_0\rho_{\rm e}}}{4a^2\widetilde{A}|\Omega|}\ln\left|\frac{(\Omega_{\rm Ae} - \Omega)(B_0K + \Omega\sqrt{\mu_0\rho_{\rm e}})}{(\Omega_{\rm Ae} + \Omega)(B_0K - \Omega\sqrt{\mu_0\rho_{\rm e}})}\right|. \quad (42)$$

This expression is valid when $\Omega^2 > 0$. If $\Omega^2 < 0$ the solution to Eq. (40) is given by

$$\xi_r = \frac{m\chi\sqrt{\mu_0\rho_{\rm e}}}{2a^2\widetilde{A}|\Omega|}\left(\arctan\frac{\Omega_{\rm Ae}}{|\Omega|} - \arctan\frac{B_0K}{|\Omega|\sqrt{\mu_0\rho_{\rm e}}}\right). \quad (43)$$

Note that $\xi_r \sim 1/r^2$ when $r \gg a$ in complete agreement with the matching conditions. Using Eq. (40) we obtain from Eq. (38) in the leading-order approximation with respect to ϵ^2 that

$$P = \frac{\epsilon^2\rho_{\rm e}\chi}{r} + \epsilon^2\, r\,\rho_{\rm e}\,\xi_r\left[\Omega^2 - \frac{1}{\mu_0\rho_{\rm e}}\left(B_0^2K^2 - \frac{a^4\widetilde{A}^2}{r^4}\right)\right]. \quad (44)$$

This equation is valid for any sign of Ω^2. In particular, it follows from this expression that $P \sim 1/r$ for $r \gg a$, which again completely agrees with the matching conditions.

3.3. Matching solutions

The solutions in the internal and external regions are related by the boundary conditions (13) and (14). Substituting expressions (30) and (42) in the boundary condition (13) we obtain the equation

$$\eta = \frac{m\chi\sqrt{\mu_0\rho_{\rm e}}}{4a^2\widetilde{A}\Omega}\ln\left|\frac{(m\widetilde{A} + B_0K - \Omega\sqrt{\mu_0\rho_{\rm e}})(B_0K + \Omega\sqrt{\mu_0\rho_{\rm e}})}{[m\widetilde{A} + B_0K + \Omega\sqrt{\mu_0\rho_{\rm e}}](B_0K - \Omega\sqrt{\mu_0\rho_{\rm e}})}\right| \quad (45)$$

which is valid for $\Omega^2 > 0$. Substituting expressions (30) and (43) in the boundary condition (13), we obtain the equation

$$\eta = \frac{m\chi\sqrt{\mu_0\rho_{\rm e}}}{2a^2\widetilde{A}|\Omega|}\left(\arctan\frac{m\widetilde{A} + B_0K}{|\Omega|\sqrt{\mu_0\rho_{\rm e}}} - \arctan\frac{B_0K}{|\Omega|\sqrt{\mu_0\rho_{\rm e}}}\right) \quad (46)$$

which is valid for $\Omega^2 < 0$. Substituting expressions (31) and (44) in the boundary condition (14) we obtain the equation

$$\eta a^2(\rho_{\rm i} - \rho_{\rm e})\Omega^2 = \rho_{\rm e}\chi. \quad (47)$$

which is valid for any sign of Ω^2. Equations (45) and (47) constitute the system of linear homogeneous equations for η and χ. It has non-trivial solutions only when its determinant is zero. This condition gives the dispersion equation

$$\omega\sqrt{\mu_0\rho_{\rm e}}\ln\left|\frac{(mA + B_0k - \omega\sqrt{\mu_0\rho_{\rm e}})(B_0k + \omega\sqrt{\mu_0\rho_{\rm e}})}{(mA + B_0k + \omega\sqrt{\mu_0\rho_{\rm e}})(B_0k - \omega\sqrt{\mu_0\rho_{\rm e}})}\right| = \frac{4m\rho_{\rm e}A}{\rho_{\rm i} - \rho_{\rm e}}, \quad (48)$$

which is valid for $\omega^2 > 0$, where $k = \epsilon K$ and $\omega = \epsilon\Omega$ are non-scaled wavenumber and frequency.

Similarly, the system of linear homogeneous equations constituted by Eqs. (46) and (47) only has non-trivial solutions when ω satisfies the dispersion equation

$$|\omega|\sqrt{\mu_0\rho_e}\left(\arctan\frac{B_0 k}{|\omega|\sqrt{\mu_0\rho_e}} - \arctan\frac{mA + B_0 k}{|\omega|\sqrt{\mu_0\rho_e}}\right) = \frac{2m\rho_e A}{\rho_i - \rho_e}. \quad (49)$$

This dispersion equation is valid for $\omega^2 < 0$. When $\rho_e < \rho_i$, it is easy to see that the left-hand side of this equation is always negative when $m = 1$, while it is always positive when $m = -1$. This implies that Eq. (49) does not have any solutions, so there are no unstable kink modes in the long-wavelength approximation. Now we consider the case where $\rho_e > \rho_i$. We rewrite Eq. (49) as $g(x) = h(x)$, where

$$g(x) = m\{\arctan[x(1 + m\sigma)] - \arctan x\},$$
$$h(x) = \frac{2\sigma\rho_e x}{\rho_e - \rho_i}, \quad \sigma = \frac{A}{B_0 k}.$$

By differentiating, we obtain

$$g'(x) = \frac{\sigma[1 - x^2(1 + m\sigma)]}{(1 + x^2)[1 + x^2(1 + m\sigma)^2]}, \quad h'(x) = \frac{2\sigma\rho_e}{\rho_e - \rho_i},$$

where the prime indicates the derivative. It is straightforward to show that $g'(x) < \sigma$, so $g'(x) < h'(x)$. Since $g(0) = h(0) = 0$, it follows that $g(x) < h(x)$. Hence, Eq. (49) does not have solutions also when $\rho_e > \rho_i$. Summarizing, we conclude that Eq. (49) does not have solutions for any sign of m and any relation between ρ_e and ρ_i. This implies that there are no unstable kink modes in the long-wavelength approximation. It is worth emphasizing that this is no complete proof of stability of the equilibrium considered in this paper. There can be unstable kink modes with a wavelength comparable with the tube radius, or unstable modes of other types.

4. Investigating the dispersion equation for propagating waves

4.1. Wave mode frequency

We introduce the quantities

$$\zeta = \frac{\rho_i}{\rho_e}, \quad V = \frac{B_0}{\sqrt{\mu_0\rho_e}}, \quad \kappa = \frac{kB_0}{A}, \quad \varpi = \frac{\omega B_0}{AV}. \quad (50)$$

Then Eq. (48) is rewritten as

$$f(\varpi) \equiv \varpi \ln\left|\frac{(m + \kappa - \varpi)(\kappa + \varpi)}{(m + \kappa + \varpi)(\kappa - \varpi)}\right| = \frac{4m}{\zeta - 1}. \quad (51)$$

It is easy to see that the left-hand side of this equation is an even function, so if ϖ is a solution to this equation then $-\varpi$ is a solution as well, which agrees with the general spectral theory of linear ideal MHD. This observation enables us to consider in our analysis $\varpi > 0$ only. We also note that

$$\varpi(\kappa; m = -1) = \varpi(-\kappa; m = 1). \quad (52)$$

In accordance with this, we take $m = 1$ below. In the dimensionless variables the condition that a wave mode is trapped given by Eq. (41) reduces to

$$\varpi < |\kappa|. \quad (53)$$

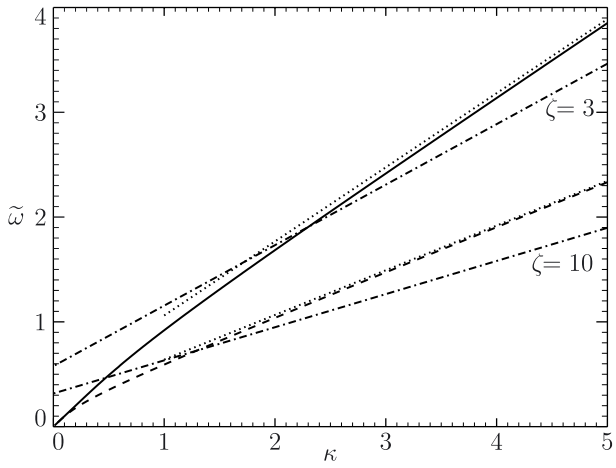

Fig. 1. Dependence of ϖ on κ for $\kappa > 0$. The solid and dashed line correspond to $\zeta = 3$ and $\zeta = 10$ respectively. The dotted lines show the approximation given by Eq. (54). The dash-dotted lines are the graphs of function $\varpi = (1 + \kappa)/\sqrt{\zeta}$ for $\zeta = 3$ and $\zeta = 10$.

The graphical investigation of Eq. (51) presented in Appendix A shows that when $\zeta > 1$, it always has exactly one positive solution that satisfies the inequality (53) when $\kappa > 0$, no real solutions when $-1 < \kappa < 0$, and two positive solutions when $\kappa < -1$.

Consider the limit of weak twist, $A \ll |k|B_0$. In the dimensionless variables this condition implies that $|\kappa| \gg 1$ and $\varpi \gg 1$. Then, assuming in addition that $|\kappa| - \varpi \gg 1$, we obtain

$$\varpi \approx \frac{|\kappa|\sqrt{2}}{\sqrt{\zeta + 1}}\left(1 + \frac{1}{2\kappa}\right). \quad (54)$$

In dimensional variables, this relation takes the form

$$\omega = C_k|k|\left(1 + \frac{A}{2kB_0}\right), \quad C_k^2 = \frac{2B^2}{\rho_i + \rho_e}, \quad (55)$$

where C_k is the kink speed. We see that in the limit of weak twist, the phase speed of the wave with $k > 0$ is higher than C_k, while the phase speed of the wave with $k < 0$ is lower than C_k. We here call the eigenmode with $k > 0$ the accelerated kink wave and the eigenmode with $k < 0$ the decelerated kink wave.

The approximate solution to the dispersion equation valid for $0 < \kappa \lesssim 1/(\zeta - 1)$ is given by

$$\varpi \approx \kappa\left[1 - \frac{2}{1 + 2\kappa}\exp\left(-\frac{4}{\kappa(\zeta - 1)}\right)\right]. \quad (56)$$

In Fig. 1 the dependence of ϖ on κ is shown for $\kappa > 0$ and two values of ζ, 3 and 10. The dotted lines show the approximation given by Eq. (54). Although this approximations was derived under the condition $|\kappa| \gg 1$, we can see that, in fact, it works for $|\kappa| \gtrsim 1$.

When $-\kappa \gg 1$, the larger of the two positive solutions to the dispersive equation that exists when $\kappa < -1$ is given by

$$\varpi \approx |\kappa| - \frac{1}{2}. \quad (57)$$

In dimensional variables this relation takes the form

$$\omega = V\left(|k| - \frac{A}{2B_0}\right). \quad (58)$$

When $0 < -\kappa - 1 \ll 1$, the two solutions to the dispersion equation are given by the approximate expression

$$\varpi \approx -(\kappa + 1)\left[1 \pm 2\exp\left(\frac{4}{(\kappa + 1)(\zeta - 1)}\right)\right]. \quad (59)$$

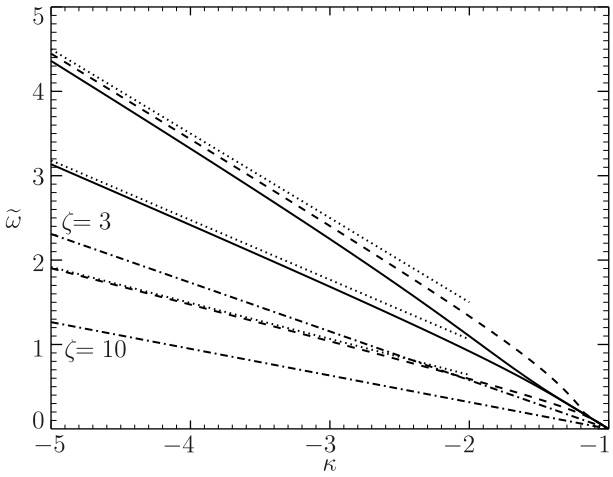

Fig. 2. Dependence of the frequency ϖ of two modes on κ for $\kappa < -1$. The solid and dashed lines correspond to $\zeta = 3$ and $\zeta = 10$. The lower dotted lines show the approximation given by Eq. (54), while the upper dotted line shows the approximation given by Eq. (57). The dashed-dotted lines are the graphs of function $\varpi = |1+\kappa|/\sqrt{\zeta}$ for $\zeta = 3$ and $\zeta = 10$.

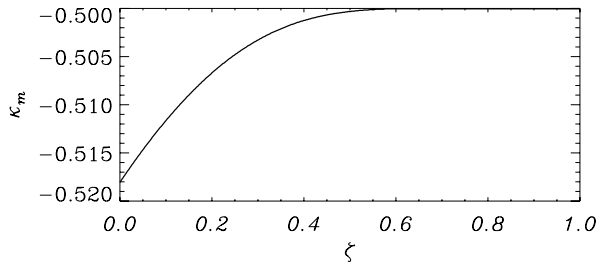

Fig. 3. Dependence of κ_m on ζ.

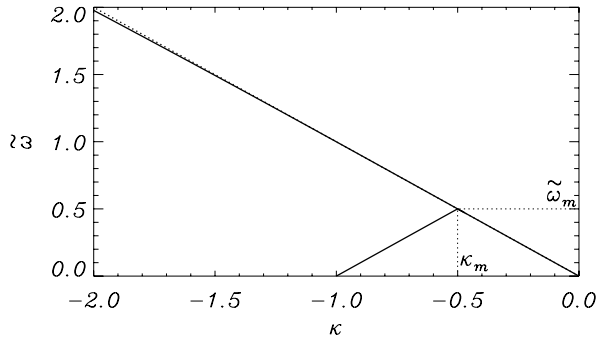

Fig. 4. Dependence of ϖ on κ for $\kappa < 0$ and $\zeta = 0.5$. The dotted line has the equation $\varpi = -\kappa$, i.e. it shows the Alfvén frequency far from the tube boundary.

The dependence of frequencies of the two wave modes on κ for $\kappa < -1$ is shown in Fig. 2.

It was assumed in Sect. 3.1 that the wave frequency does not coincide with the internal Alfvén frequency. In the dimensionless variables the internal Alfvén frequency is

$$\varpi_{\rm Ai} = \frac{|1+\kappa|}{\sqrt{\zeta}}. \tag{60}$$

Figure 1 shows that ϖ is a monotonically increasing function of κ for $\kappa > 0$, and, at $\kappa = 0$, $\varpi = 0$ while $\varpi_{\rm Ai} = 1/\sqrt{\zeta}$. On the other hand, it follows from Eqs. (54) and (60) that $\varpi > \varpi_{\rm Ai}$ for $\kappa \gg 1$. Hence, there is a value $\kappa_{\rm Ai}$ that $\varpi = \varpi_{\rm Ai}$ at $\kappa = \kappa_{\rm Ai}$. At this value of κ, there should be strong interaction between the kink mode and the internal Alfvén wave.

Now we investigate if an eigenmode frequency can coincide with the external Alfvén frequency, which is given in the dimensionless variables by $\varpi_{\rm Ae} = |a^2/r^2 + \kappa|$. When $\kappa > 0$, $\varpi_{\rm Ae} > \kappa$, while, for trapped waves, $\varpi < \kappa$. Hence, $\varpi < \varpi_{\rm Ae}$ and the eigenmode frequency cannot coincide with the external Alfvén frequency.

Consider now $\kappa < 0$. Since propagating modes only exist when $\kappa < -1$, we obtain $\varpi_{\rm Ae} = -a^2/r^2 - \kappa$. Then it follows that

$$-\kappa - 1 < \varpi_{\rm Ae} < -\kappa. \tag{61}$$

Since the eigenfrequency of the decelerated wave mode is lower than $-\kappa - 1$, we conclude that it is lower than $\varpi_{\rm Ae}$. On the other hand, $\varpi_{\rm Ae}$ monotonically increases from $-\kappa - 1$ to $-\kappa$ when r increases from a to ∞. Since the frequency of the second mode that exists when $\kappa < -1$ is between $-\kappa - 1$ and $-\kappa$, we conclude that there is $r_{\rm A}$ such that the frequency of this mode coincides with $\varpi_{\rm Ae}$ at $r = r_{\rm A}$, meaning that there is an Alfvén-resonant position for this kink mode. This implies that this kink mode is not an eigenmode, but a quasi-mode. Because the Alfvén resonance, it damps, therefore its frequency is complex. Its real part is approximately defined by the dispersion Eq. (48) only when the damping is weak. We did not investigate the resonant damping of this kink mode. It will be the a subject of the future study.

Now we consider the case where $\rho_{\rm e} > \rho_{\rm i}$. It is proved in Appendix A that in this case there are no trapped modes when $\kappa > 0$, there is exactly one trapped mode when $\kappa_m(\zeta) < \kappa < 0$, three trapped modes when $-1 < \kappa < \kappa_m(\zeta)$, and again exactly one trapped mode when $\kappa < -1$. The dependence of κ_m on ζ is shown in Fig. 3. In Fig. 4 the dependence of frequencies of trapped modes on κ is shown for $\kappa < 0$ and $\zeta = 0.5$.

When $|\kappa| \gg 1$ and $\kappa < 0$, the frequency of the trapped mode is given by the approximate expression

$$\varpi = -\kappa - \frac{1}{2}. \tag{62}$$

When $0 < \kappa + 1 \ll 1$, the two lower trapped eigenmode frequencies are given by the approximate expression

$$\varpi = (\kappa+1)\left[1 \pm 2\exp\left(\frac{-4}{(1-\zeta)(1+\kappa)}\right)\right]. \tag{63}$$

Finally, when $\kappa < 0$ and $|\kappa| \ll 1$, the eigenfrequency is given by

$$\varpi = -\kappa\left[1 - 2\exp\left(\frac{4}{\kappa(1-\zeta)}\right)\right]. \tag{64}$$

It is also easy to obtain the approximate expressions for κ_m and for the corresponding double root of the dispersion equation, ϖ_m,

$$\kappa_m \approx -\frac{1}{2} - \exp\left(-\frac{4}{1-\zeta}\right), \tag{65}$$

$$\varpi_m \approx \frac{1}{2} - \frac{17-\zeta}{1-\zeta}\exp\left(-\frac{8}{1-\zeta}\right). \tag{66}$$

Note that the value given by Eq. (65) coincides with the numerically calculated value presented in Fig. 3 with very high accuracy for all values of $\zeta < 1$.

When κ is close to κ_m the two larger roots of the dispersion equation are given by the approximate formula

$$\varpi \approx \varpi_m \pm \exp\left(-\frac{2}{1-\zeta}\right)\sqrt{\kappa_m - \kappa}. \tag{67}$$

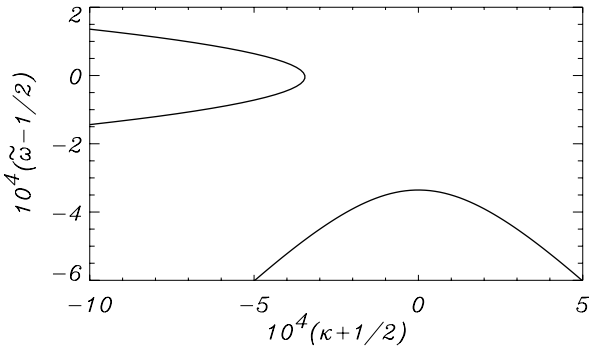

Fig. 5. Zoomed dependence of ϖ on κ for $\kappa < 0$ and $\zeta = 0.5$.

This approximate expression is only valid when $|\varpi - \varpi_m| \ll 1$, which is equivalent to the condition

$$\kappa_m - \kappa \ll \exp\left(-\frac{4}{1-\zeta}\right). \tag{68}$$

Hence, Eq. (67) is only valid in a very close vicinity of κ_m.

When $\zeta = 0.5$, we have $\kappa_m \approx -0.500335 \approx -0.5$ and $\varpi_m \approx 0.499996 \approx 0.5$. We see in Fig. 4 that the dispersion curves are almost straight lines. We denote the frequency of the wave mode that exits when $-1 < \kappa < 0$ as ϖ_1, the frequency of the wave mode that exits only when $-1 < \kappa < \kappa_m$ as ϖ_2, and the frequency of the wave mode that exits when $\kappa < \kappa_m$ as ϖ_3. The dispersion curve $\varpi = \varpi_2(\kappa)$ connects the points $(-1, 0)$ and (κ_m, ϖ_m) in the $\kappa\varpi$-plane. This curve is slightly above the curve $\varpi = \varpi_1(\kappa)$, but the difference between ϖ_1 and ϖ_2 is so small, however, that these two curves are indistinguishable when $-1 < \kappa < \kappa_m$. The apex point of the curve $\varpi = \varpi_1(\kappa)$ is $(-0.5, 0.5)$, while the curve $\varpi = \varpi_3(\kappa)$ starts from the point (κ_m, ϖ_m). The distance between the points $(-0.5, 0.5)$ and (κ_m, ϖ_m) is so small that the second curve looks like the continuation of the first one. To better reveal the behaviour of dispersion curves we zoomed the vicinity of point $(-0.5, 0.5)$ in Fig. 5.

The dotted curve has the equation $\varpi = -\kappa$, meaning that it shows the Alfvén frequency far from the tube boundary. We see that it almost indistinguishable from the curves $\varpi = \varpi_1(\kappa)$ and $\varpi = \varpi_2(\kappa)$, which means that the frequencies of these modes are very close to the Alfvén frequency far from the tube. This means that these modes are very close to Alfvén waves with $m = \pm 1$ that can exist far from the tube where the Alfvén speed is almost constant. Although from the formal mathematical point of view, modes with frequencies ϖ_1 and ϖ_2 are trapped modes, the bulk of their energy is contained far from the tube, therefore physically they do not look like trapped modes. Note that the qualitative behaviour of the dispersion curves is the same for any $\zeta < 1$.

Finally, we prove that all trapped wave modes that exists when $\zeta < 1$ are, in fact, quasi-modes and subject to resonant absorption. For the external Alfvén frequency we have $\varpi_{Ae} = |a^2/r^2 + \kappa|$. We see that $\varpi_{Ae} = |1 + \kappa|$ when $r = a$. When $\kappa > -1$, ϖ_{Ae} monotonically decreases when r increases and takes its minimum equal to zero at $r = r/\sqrt{-\kappa}$. Then it monotonically increases when r increases further and tends to $-\kappa$ as $r \to \infty$. Since for all trapped modes $\varpi < -\kappa$, the frequency of any such mode is equal to the external Alfvén frequency at some value of r when $\kappa > -1$.

When $\kappa < -1$, the external Alfvén frequency monotonically increases from $-\kappa - 1$ to $-\kappa$ when r increases from a to infinity. Since the frequency of the only trapped mode that exists in this case is between $-\kappa - 1$ and $-\kappa$, it is again obvious that this frequency is equal to the external Alfvén frequency at some value of r.

Finally, we discuss the relation between the properties of propagating waves in straight and twisted tubes. Trapped wave modes do not exist in a magnetic tube where the density inside the tube is lower than that in the surrounding plasma (e.g. Ruderman & Roberts 2006). We obtain a straight tube taking $A \to 0$, which corresponds to $\kappa \to \infty$. The frequency of the single mode that exists when $\kappa < -1$ tends to the Alfvén frequency far from the tube, and thus this mode is no longer trapped. Hence, the results obtained for a twisted tube agree with those obtained for a straight tube.

4.2. Wave mode polarization

In this section we study the polarization of wave modes. Since all trapped modes are quasi-modes when $\zeta < 1$, we restrict our analysis to $\zeta > 1$. First of all, we note that in the leading-order approximation with respect to ϵ, we have $\xi_\varphi = \xi_\perp$, $\xi_z = 0$, and $\xi_\perp$ is related to ξ_r by Eq. (26). Then we have inside the tube

$$\xi_r = \eta \exp[\mathrm{i}(\varphi + kz - \omega t)], \quad \xi_\varphi = \mathrm{i}\eta \exp[\mathrm{i}(\varphi + kz - \omega t)], \tag{69}$$

where, without loss of generality, we can take η real. Below we only consider waves propagating in the positive z-direction, so we take $\omega > 0$ when $k > 0$, and $\omega < 0$ when $k < 0$ (we recall that if ω is a solution to the dispersion equation, then $-\omega$ is also a solution). Since $\omega(k; m = -1) = \omega(-k; m = 1)$, we have the second eigenmode solution

$$\xi_r = \eta \exp[-\mathrm{i}(\varphi + kz - \omega t)], \quad \xi_\varphi = -\mathrm{i}\eta \exp[-\mathrm{i}(\varphi + kz - \omega t)], \tag{70}$$

where, in accordance with our agreement, we substituted $-\omega$ for ω. The superposition of these two solutions gives the real solution

$$\xi_r = \eta \cos(\varphi + kz - \omega t), \quad \xi_\varphi = -\eta \sin(\varphi + kz - \omega t). \tag{71}$$

We immediately see that the length of the displacement vector does not change and is equal to η, so the wave mode is circularly polarized. Now we introduce auxiliary Cartesian coordinates x, y, z with the same z-axis as in the cylindrical coordinates. Then for the components of the projection of the displacement vector on the xy-place we have

$$\xi_x = \eta \cos(\omega t - kz), \quad \xi_y = \eta \sin(\omega t - kz). \tag{72}$$

First we consider the wave mode with $k > 0$, so in accordance with our agreement, $\omega > 0$. In accordance with Eq. (54), in the long-wavelength approximation, the phase speed of this wave is higher than C_k. At a fixed z the displacement vector rotates with the angular velocity ω in the counter-clockwise direction. Hence, this is a right-hand polarized wave as defined from the point of view of the source.

For modes with $k < 0$ the situation is just the opposite. In accordance with Eq. (54), in the long-wavelength approximation, the phase speed of this wave is lower than C_k. Since $\omega < 0$, at a fixed z, the displacement vector rotates with the angular velocity $|\omega|$ in the clockwise direction. Hence, this is a left-hand polarized wave as defined from the point of view of the source.

The situation here is quite similar to that with circularly polarized waves propagating along the magnetic field in a Hall plasma. These waves propagate with the Alfvén speed in the

very long-wavelength approximation. When the dispersion correction in the long-wavelength approximation is taken into account, the phase speed of the right-hand polarized wave is slightly higher than the Alfvén speed, while the phase speed of the left-hand polarized wave is slightly lower than the Alfvén speed (see, e.g. Ruderman & Caillol 2008, and references therein).

We now discuss the relation between the properties of kink waves and their polarization from somewhat different point of view. The equation of magnetic field lines is

$$\frac{r\,\mathrm{d}\varphi}{B_\varphi} = \frac{\mathrm{d}z}{B_z}, \tag{73}$$

and any field line is situated on a cylindrical surface $r = \text{const}$. In particular, at the tube boundary, where $B_z = B_0$ and $B_\varphi = aA$, the equations of any field line are

$$r = a, \quad z = \frac{B_0}{A}\varphi + \text{const}. \tag{74}$$

This is the equation of a right-hand helix of radius a and pitch $2\pi B_0/A$.

We now consider the hodograph of vector $\boldsymbol{h} = (\xi_x, \xi_y, z)$ obtained at fixed t by varying z from $-\infty$ to ∞. We take the vector $\boldsymbol{\xi}$ to be inside the tube, so its components are given by Eq. (72). As a result we obtain a left-hand helix when $k > 0$, that is, when the wave is accelerated, and a right-hand helix when $k < 0$, that is, when the wave is decelerated. Both helices are of radius η and pitch $2\pi/|k| = l$. Since there are accelerated waves with any $k > 0$, an accelerated wave with any pitch of the hodograph of vector $\boldsymbol{h}$ can propagate. On the other hand, a decelerated wave can only propagate when $k < -A/B_0$, that is, when the pitch of the hodograph of vector $\boldsymbol{h}$ is smaller than the pitch of any magnetic field line on the tube surface.

We assumed from the very beginning that $A > 0$, which means that all the magnetic field lines are right-hand helices. We now consider the case where $A < 0$, so all the magnetic field lines are left-hand helices. In this case the analysis remains almost the same. The only difference is that in this case, the accelerated wave is left-hand polarized, and the decelerated wave is right-hand polarized.

We give one example. We consider the kink wave propagation along a coronal loop. Let the component of the equilibrium magnetic field that is orthogonal to the loop axis rotate by the angle α when we move from one loop foot point to the other. In particular, $\alpha = 2\pi$ corresponds to the full turn of the magnetic field line. In accordance with Eq. (74) we have the relation $A/B_0 = \alpha/L$, where L is the loop length. Using this result we obtain the relation $\kappa = 2\pi L/\alpha l$ (recall that l is the wavelength). Obviously, the analysis of this paper can only be used for waves with $l \ll L$. Then, assuming that the twist is not very strong either, $\alpha \lesssim 2\pi$, we obtain $\kappa \gg 1$. This implies that we can use the approximate formula (55) for the frequencies of the accelerated and decelerated wave. Then we obtain that the ratio of their frequencies is approximately equal to

$$\frac{\omega_\mathrm{a}}{\omega_\mathrm{d}} = 1 + \frac{2\alpha l}{\pi L}, \tag{75}$$

where ω_a and ω_d are the frequencies of the accelerated and decelerated kink wave. Even for quite short waves with l of the order of $L/10$, the frequencies can differ by as much as 40% when there is a substantial magnetic twist in the loop with $\alpha \simeq 2\pi$.

Up to now, no observations have been reported of two kink waves that simultaneously propagate along a magnetic wave guide. Quite possibly, that the magnetic twist in wave guides in the solar atmosphere is always very low and, as a result, the accelerated and decelerated wave have almost the same phase speed. Another explanation is that perturbations propagating with different phase speeds in magnetic wave guides have not been searched for in observational data. The results obtained here may prompt researchers dealing with observations to search for such perturbations. If simultaneously propagating kink waves with different phase speeds are observed, then this might be very useful from the point of view of solar atmospheric seismology because such an observation could be used to estimate the angle of the magnetic twist α using Eq. (75).

5. Summary and conclusions

We have studied the propagation of kink waves in twisted magnetic tubes. It was assumed that in the equilibrium state, there is electrical current with constant density inside the tube directed along the tube axis. This current creates the azimuthal component of the magnetic field with the magnitude proportional to the distance from the tube axis inside the tube and inversely proportional to this distance outside the tube. The plasma density was assumed to be constant inside and outside the tube. The analysis was carried out in the long-wavelength approximation, that is, under the assumption that the wavelength is much larger than the tube radius.

In accordance with the general spectral theory of linear MHD the eigenfrequencies of wave modes can be either real or purely imaginary. The modes with the real frequency are propagating waves, while those with purely imaginary frequencies are either damped or growing perturbations. We derived the dispersion equations for the two cases separately (see Eqs. (48) and (49)). We showed that the dispersion equation for modes with purely imaginary frequency does not have any solutions. This implies that there are no unstable kink modes in the long-wavelength approximation.

When the plasma density inside the tube is higher than that in the surrounding plasma, the investigation of the dispersion equation for propagating waves showed that there are three distinctive wave number intervals. In the first interval exactly one wave mode is trapped. Because in the approximation of weak twist the phase speed of this mode is higher than the kink speed, we called this wave mode the accelerated kink wave. In the second interval the dispersion equation does not have any solutions, so there are no propagating waves with wavenumbers from this interval. In the third interval the dispersion equation has two solutions. The wave mode with the higher frequency is a quasi-mode because its frequency is in the external Alfvén continuum and is subjected to the Alfvén resonance. Hence, its frequency is complex. The real part of its frequency is approximately determined by the dispersion equation only when the damping due to Alfvén resonance is weak. The wave mode with the lower frequency is a true wave mode of linear ideal MHD. In the approximation of weak twist, the phase speed of this mode is lower than the kink speed. This inspired us to call this wave mode the decelerated kink wave.

We also studied the case where the plasma density inside the tube is lower than that in the surrounding plasma. In this case the trapped modes only exist when the wave number is negative, so the wave number can vary from zero to minus infinity. The interval of the wave number variation can be divided into three subintervals, the thirst subinterval being semi-infinite. When the wave number is either in the first or in the third subinterval, there is exactly one trapped mode. This mode frequency is very close

to the external Alfvén frequency far from the tube axis. The bulk of the energy of this mode is in the region far from the tube boundary. Hence, although from the formal mathematical point of view, this mode can be called trapped, its physical properties do not resemble the characteristics of trapped modes.

When the wave number is in the second subinterval, there are three trapped wave modes. The frequency of the first mode is again very close to the external Alfvén frequency far from the tube axis. The frequencies of the two other modes are very close to each other. Finally, all wave modes are, in fact, quasi-modes and must be subject to damping as a result of resonant absorption.

To study the propagating kink waves, we used a relatively simple model of a magnetic tube with the constant electrical current density inside the tube and a current-free environment. The assumption that the environment is current-free, so that the current is only concentrated inside the tube, seems to be quite general. If it is satisfied, then the equilibrium magnetic field outside the tube is independent of a particular distribution of the electrical current inside the tube. Its axial component is constant, and the azimuthal component is inversely proportional to the distance from the tube axis. If the current density inside the tube varies in the radial direction, then the local Alfvén frequency will also vary in the radial direction, and we can expect wave damping as a result of resonant absorption. However, we can expect that the propagation properties of the waves will remain qualitatively the same. In particular, if the plasma density inside the tube is higher than that of the surrounding plasma, one can expect that there will be two modes with opposite polarization that propagate with different phase speeds.

We also comment on the relation between propagating and standing waves. In a magnetic tube with straight magnetic field lines a standing wave is a superposition of two identical propagating waves travelling in the opposite directions. The presence of magnetic twist destroys the invariance of the equilibrium with respect to changing the tube axis direction. For a particular equilibrium as considered in Paper I, however, a standing wave is still a superposition of two propagating waves. The only difference in comparison with a tube with straight magnetic field lines is that now the two propagating waves have the same frequency but different wave numbers.

The situation is completely different for the equilibrium considered in this article. The solution in the external region is not factorized, meaning that it cannot be written as a product of the function of r that is independent of the wave number and a multiplier that depends on the wave number (see Eqs. (42) and (44)). As a result, a superposition of two or even a few propagating waves cannot satisfy the frozen-in boundary conditions at the loop footpoints in the external region. Studying standing waves is a much more difficult problem than studying propagating waves. It should be solved without the Fourier analysis with respect to z, so the governing equations cannot be reduced to ordinary differential equations. This implies that there is no obvious relation between standing and propagation waves, and we cannot conclude about the properties of standing waves on the basis of analysing propagating waves.

Acknowledgements. A part of this work was carried out when MSR was a guest of Departament de Física of Universitat de les Illes Balears. He acknowledges the financial support received from the Universitat de les Illes Balears and the warm hospitality of the Departament. He also acknowledges the support by the STFC grant, and by the Russian Fund for Fundamental Research (RFBR) grant (13-02-00656).

References

Aschwanden, M. J., Fletcher, L., Schrijver, C. J., & Alexander, D. 1999, ApJ, 520, 880
Ballay, I., & Erdélyi, R. 2002, J. Plasma Phys., 67, 79
Bennett, K., Roberts, B., & Narain, U. 1999, Sol. Phys., 185, 41
Bogdan, T. J. 1984, ApJ, 282, 769
Browning, P. K., & Priest, E. R. 1983, ApJ, 266, 848
Carter, P. S., & Erdélyi, R. 2007, A&A, 475, 323
De Pontieu, B., McIntosh, S. W., Carlsson, M., et al. 2007, Science, 318, 1574
Dungey, J. W., & Loughead, R. E. 1954, Austr. J. Phys., 7, 5
Edwin, P. M., & Roberts, B. 1983, Sol. Phys., 88, 179
Erdélyi, R., & Carter, B. K. 2006, A&A, 455, 361
Erdélyi, R., & Fedun, V. 2007, Sol. Phys., 246, 101
Goedbloed, J. P. H., & Poedts, S. 2004, Principles of Magnetohydrodynamics (Cambridge, UK: Cambridge University Press)
Goossens, M., & Ruderman, M. S. 1995, Phys. Scr., 60, 171
Goossens, M., Ruderman, M. S., & Hollweg, J. V. 1995, Sol. Phys., 157, 75
Goossens, M., Van Doorsselaere, T., Soler, R., & Verth, G. 2013, ApJ, 768, A191
Goossens, M., Soler, R., Terradas, J., Van Doorsselaere, T., & Verth, G. 2014, ApJ, 788, A9
He, J.-S., Marsch, E., Tu, C.-Y., Guo, L. J., & Tian, H. 2009a, ApJ, 705, L217
He, J.-S., Tu, C.-Y., Marsch, E., et al. 2009b, A&A, 497, 525
Hood, A.-W., Ruderman, M.-S., Pascoe, D. J., et al. 2013, A&A, 551, A39
Kruskal, M., & Tuck, J. L. 1958, Proc. R. Soc. London A, 245, 222
Lin, Y., Engvold, O., Rouppe van der Voort, L. H. M., & van Noort, M. 2007, Sol. Phys., 246, 65
Lin, Y., Solar, R., Engvold, O., et al. 2009, ApJ, 704, 870
Morton, R., Verth, G., Jess, D. V., et al. 2012, Nature Commun., 3, 1315
Nakariakov, V. M., Ofman, L., Deluca, E. E., Roberts, B., & Davila, J. M. 1999, Science, 285, 862
Okamoto, T. J., Tsuneta, S., Berger, T. E., et al. 2007, Science, 318, 1591
Parker, E. N. 1974, ApJ, 191, 245
Pascoe, D. J., Wright, A. N., & De Moortel, I. 2010, ApJ, 711, 990
Pascoe, D. J., Wright, A. N., & De Moortel, I. 2011, ApJ, 731, 73
Pascoe, D. J., Wright, A. N., De Moortel, I., & Wright, A. N. 2012, A&A, 539, A37
Roberts, P. H. 1956, ApJ, 124, 430
Ruderman, M. S. 2007, Sol. Phys., 246, 119
Ruderman, M. S., & Caillol, P. 2008, J. Plasma Phys., 74, 119
Ruderman, M. S., & Erdélyi, R. 2009, Space Sci. Rev., 149, 199
Ruderman, M. S., & Roberts, B. 2006, J. Plasma Phys., 72, 285
Ruderman, M. S., Goossens, M., & Andries, J. 2010, Phys. Plasmas, 17, A082108
Ryutov, D. D., & Ryutova, M. P. 1976, JETP, 43, 491
Sakurai, H., Goossens, S., & Hollweg, Y. 1991, Sol. Phys., 133, 227
Shafranov, V. D. 1957, J. Nucl. Energy II, 5, 86
Soler, R., Terradas, J., Verth, G., & Goossens, M. 2008, ApJ, 736, A10
Terradas, J., & Goossens, M. 2012, A&A, 548, A112
Terradas, J., Goossens, M., & Verth, G. 2010, A&A, 524, A23
Tomczyk, S., & McIntosh, S. W. 2009, ApJ, 697, 1384
Tomczyk, S., McIntosh, S. W., Keil, S. L., et al. 2007, Science, 317, 1192

Pages 10 to 11 are available in the electronic edition of the journal at http://www.aanda.org

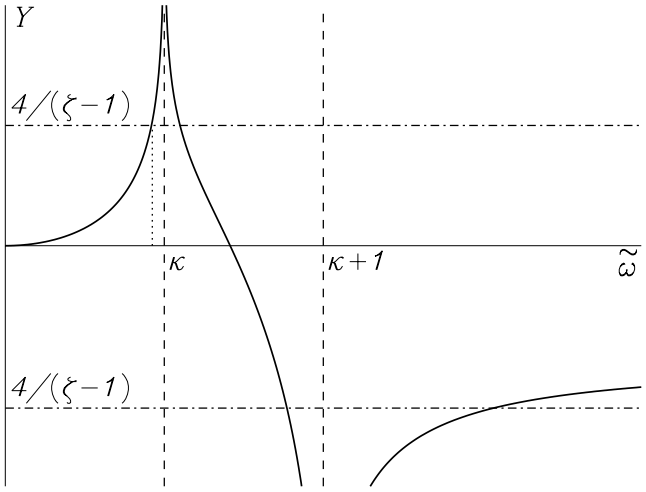

Fig. A.1. Graphical investigation of the dispersion equation for $\kappa > 0$. The solid lines show the graph of function $Y = f(\varpi)$, while the dashed lines have equations $Y = 4/(\zeta - 1)$. The upper dashed-dotted line corresponding to $\zeta > 1$ intersects the solid lines at two points corresponding to two roots to the dispersion equation. However, only one of these roots satisfies the condition $\varpi < |\kappa|$. The vertical dotted line indicates the root satisfying the condition $\varpi < |\kappa|$. The lower dashed-dotted line corresponding to $\zeta < 1$ intersects the solid lines at two points corresponding to roots of the dispersion equation. However, none of them satisfies the condition $\varpi < |\kappa|$.

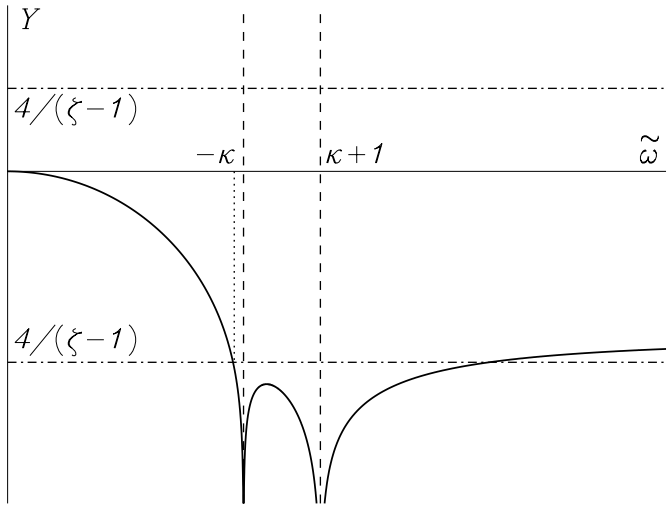

Fig. A.2. Graphical investigation of the dispersion equation for $-\frac{1}{2} < \kappa < 0$. The solid lines show the graph of function $Y = f(\varpi)$, while the dashed-dotted lines have equations $Y = 4/(\zeta - 1)$. The upper dashed-dotted line corresponding to $\zeta > 1$ does not intersect the solid lines, which implies that there are no propagating wave modes when $-\frac{1}{2} < \kappa < 0$. Depending on the value of $\zeta < 1$, the lower dashed-dotted line intersects the solid lines either at two or at four points, so there are up to four positive roots of the dispersion equation. However, only one of them satisfies the condition $\varpi < |\kappa|$. The vertical dotted line indicates the root satisfying the condition $\varpi < |\kappa|$.

Appendix A: Graphical investigation of the dispersion equation

In this section we present the graphical investigation of the dispersion equation. We start from the case where $\zeta > 1$. In Fig. A.1 the graph of function $Y = f(\varpi)$ is shown for $\kappa > 0$. The upper horizontal line $Y = 4/(\zeta - 1)$ corresponding to $\zeta > 1$ crosses this graph twice, so there are two positive roots to Eq. (51). However, only one of them satisfies the inequality (53). Hence, there is only one trapped wave mode with positive frequency when $\kappa > 0$.

In Fig. A.2 the graph of function $Y = f(\varpi)$ is shown for $-\frac{1}{2} < \kappa < 0$. Now the upper horizontal line $Y = 4/(\zeta - 1)$ does not cross the graph of function $Y = f(\varpi)$. Hence, there are no roots of Eq. (51) when $-\frac{1}{2} < \kappa < 0$. In Fig. A.3 the graph of function $Y = f(\varpi)$ is shown for $-1 < \kappa < -\frac{1}{2}$. Again the upper horizontal line $Y = 4/(\zeta - 1)$ does not cross the graph of function $Y = f(\varpi)$. Hence, there are no roots of Eq. (51) when $-1 < \kappa < -\frac{1}{2}$. Summarizing, we conclude that there are no propagating wave modes when $-1 < \kappa < 0$.

Finally, Fig. A.4 displays the graph of function $Y = f(\varpi)$ for $\kappa < -1$. It is quite similar to Fig. A.1. In particular, the upper horizontal line $Y = 4/(\zeta - 1)$ again crosses the graph of function $Y = f(\varpi)$ twice, so there are two positive roots to Eq. (51). However, now both roots satisfy the inequality (53). Hence, there are two trapped wave modes with positive frequency when $\kappa < -1$ but, as is shown in Sect. 4.1, the wave with the higher frequency is a quasi-mode that is subject to resonance absorption.

Now we proceed to studying the case where $\zeta < 1$. Since now $4/(\zeta - 1) < -4$, while $f(\varpi) \to -1$ as $\varpi \to \infty$, in Fig. A.1 the lower horizontal line $Y = 4/(\zeta - 1)$ corresponding to $\zeta < 1$ crosses the graph of function $Y = f(\varpi)$ twice, so there are two positive roots of Eq. (51). However, none of them satisfies the inequality (53). Hence, there are no trapped wave modes when $\kappa > 0$.

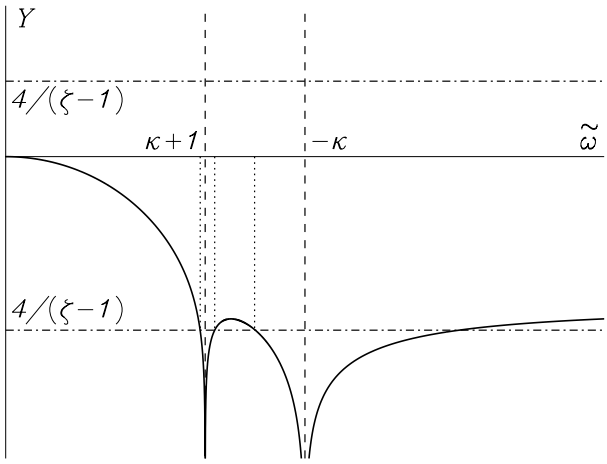

Fig. A.3. Graphical investigation of the dispersion equation for $-1 < \kappa < -\frac{1}{2}$. The solid lines show the graph of function $Y = f(\varpi)$, while the dashed-dotted lines have equations $Y = 4/(\zeta - 1)$. The upper dashed-dotted line corresponding to $\zeta > 1$ does not intersect the solid lines, which implies that there are no propagating wave modes when $-1 < \kappa < -\frac{1}{2}$. Depending on the value of $\zeta < 1$, the lower dashed-dotted line intersects the solid lines either at two or at four points, so there are up to four positive roots of the dispersion equation. The root corresponding to the intersection with the right branch of graph of function $Y = f(\varpi)$ does not satisfy the condition $\varpi < |\kappa|$, while all other roots satisfy this condition. The vertical dotted lines indicate the roots satisfying the condition $\varpi < |\kappa|$.

Depending on the value of $\zeta < 1$, the lower horizontal line $Y = 4/(\zeta - 1)$ in Fig. A.2 can cross the graph of function $f(\varpi)$ either two or four times. Hence, there can be up to four positive roots to Eq. (51). However, only one of them satisfies the

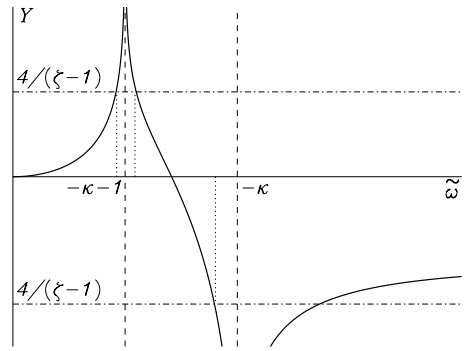

Fig. A.4. Graphical investigation of the dispersion equation for $\kappa < -1$. The solid lines show the graph of function $Y = f(\varpi)$, while the dashed lines have equations $Y = 4/(\zeta - 1)$. The upper dashed-dotted line corresponding to $\zeta > 1$ intersects the solid lines at two points corresponding to two roots to the dispersion equation. Both these roots satisfy the condition $\varpi < |\kappa|$. The lower dashed-dotted line intersects the solid lines at two points, so there are two positive roots. But only the smaller root satisfies the condition $\varpi < |\kappa|$. The vertical dotted lines indicate the roots satisfying the condition $\varpi < |\kappa|$.

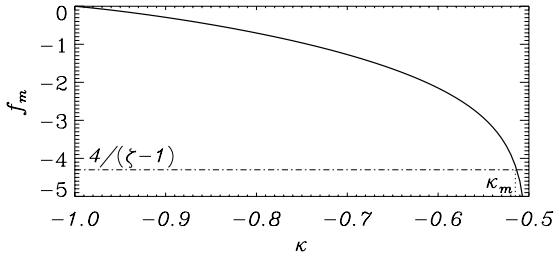

Fig. A.5. Dependence of f_m on κ is shown by the solid line. The horizontal dashed-dotted line shows $f_m = 4/(\zeta - 1)$, and the vertical dotted line indicates κ_m.

inequality (53). Hence, there is exactly one trapped wave mode with the positive frequency when $-\frac{1}{2} < \kappa < 0$.

In Fig. A.3 the graph of function $Y = f(\varpi)$ is shown for $-1 < \kappa < -\frac{1}{2}$. For $\varpi > 0$ this graph consists of three branches. An intersection of the horizontal line $Y = 4/(\zeta - 1)$ with the right branch corresponds to a root that does not satisfy the inequality (53). The horizontal line intersects the left branch for any value $\zeta < 1$. The corresponding root of Eq. (51) satisfies the inequality (53) and thus it is the frequency of a trapped mode. We denote the maximum value of function $f(\varpi)$ in the interval $(\kappa + 1, -\kappa)$ as $f_m(\kappa)$. This function monotonically decreases from 0 to $-\infty$ when κ varies from -1 to $-\frac{1}{2}$. The dependence of f_m on κ is shown in Fig. A.5. When $4/(\zeta-1) > f_m(\kappa)$ the dashed-dotted line does not intersect the middle branch, so in this case there is only one trapped wave mode. Otherwise there are three trapped wave modes. We see in Fig. A.5 that the condition $4/(\zeta - 1) > f_m(\kappa)$ is satisfied when $\kappa \in (\kappa_m, -\frac{1}{2})$, and it is not satisfied when $\kappa \in (-1, \kappa_m)$. Hence, there are three trapped wave modes when $\kappa \in (-1, \kappa_m)$, and only one when $\kappa \in (\kappa_m, -\frac{1}{2})$. The dependence of κ_m on ζ is shown in Fig. 3.

Finally, in Fig. A.4 the graph of function $Y = f(\varpi)$ is shown for $\kappa < -1$. The horizontal line intersects this graph at two points. But only the smaller root satisfies the condition $\varpi < |\kappa|$.

Appendix B: Proof that the frequencies of the decelerated kink wave and the quasi-mode do not coincide with the internal Alfvén frequency

In this section we prove that the frequencies of the two trapped wave modes that exist when $\zeta > 1$ and $\kappa < -1$ do not coincide with the internal Alfvén frequency. We can see in Fig. A.3 that the function $f(\varpi)$ is monotonically increasing in the interval $(0, -\kappa - 1)$. Let us prove that

$$f(\varpi_{\rm Ai}) < \frac{4}{\zeta - 1}. \tag{B.1}$$

This inequality can be rewritten as

$$g(\kappa) \equiv \ln\left|\frac{(\sqrt{\zeta}+1)(\sqrt{\zeta}\kappa - \kappa - 1)}{(\sqrt{\zeta}-1)(\sqrt{\zeta}\kappa + \kappa + 1)}\right| < -\frac{4\sqrt{\zeta}}{(\zeta-1)(\kappa+1)}. \tag{B.2}$$

We have

$$\frac{{\rm d}g}{{\rm d}\kappa} = \frac{2\sqrt{\zeta}}{\zeta\kappa^2 - (\kappa+1)^2} > 0 \tag{B.3}$$

because $\zeta > 1$ and $-\kappa - 1 < -\kappa$. Hence, $g(\kappa)$ is a monotonically increasing function. For $|\kappa| \gg 1$

$$g(\kappa) = -\frac{2\sqrt{\zeta}}{(\zeta-1)\kappa} + O(|\kappa|^{-2}) < -\frac{4\sqrt{\zeta}}{(\zeta-1)(\kappa+1)}. \tag{B.4}$$

Since $g(\kappa)$ is monotonically increasing, this result implies that the inequality (B.2) is correct for any $\kappa < -1$. Then the same is true for the inequality (B.1), which can be rewritten as

$$f(\varpi_{\rm Ai}) < f(\varpi_-). \tag{B.5}$$

Since $f(\varpi)$ is monotonically increasing in the interval $(0, -\kappa-1)$, this inequality implies that $\varpi_{\rm Ai} < \varpi_-$. Since $\varpi_- < \varpi_+$, it follows that also $\varpi_{\rm Ai} < \varpi_+$.